Analytical description of spin-Rabi oscillation controlled electronic transitions rates between weakly coupled pairs of paramagnetic states with $S = \frac{1}{2}$

R. Glenn, W. J. Baker, C. Boehme, and M. E. Raikh
Department of Physics and Astronomy, University of Utah, Salt Lake City, Utah 84112, USA
(Received 30 July 2012; revised manuscript received 13 November 2012; published 19 April 2013)

We report on the theoretical and experimental study of spin-dependent electronic transition rates which are controlled by a radiation-induced spin-Rabi oscillation of weakly spin-exchange and spin-dipolar coupled paramagnetic states ($S = \frac{1}{2}$). The oscillation components [the Fourier content, $\mathbf{F}(s)$] of the net transition rates within spin-pair ensembles are derived for randomly distributed spin resonances, with an account of a possible correlation between the two distributions corresponding to individual pair partners. Our study shows that when electrically detected Rabi spectroscopy is conducted under an increasing driving field B_1, the Rabi spectrum, $\mathbf{F}(s)$, evolves from a single peak at $s = \Omega_R$, where $\Omega_R = \gamma B_1$ is the Rabi frequency (γ is the gyromagnetic ratio), to *three* peaks at $s = \Omega_R$, $s = 2\Omega_R$, and low $s \ll \Omega_R$. The crossover between the two regimes takes place when Ω_R exceeds the expectation value δ_0 of the difference in the Zeeman energies within the pairs, which corresponds to the broadening of the magnetic resonance by disorder caused by a hyperfine field or distributions of Landé g factors. We capture this crossover by analytically calculating the shapes of all three peaks at an arbitrary relation between Ω_R and δ_0. When the peaks are well developed their widths are $\Delta s \sim \delta_0^2/\Omega_R$. We find a good quantitative agreement between the theory and experiment.

DOI: 10.1103/PhysRevB.87.155208 PACS number(s): 42.50.Md, 76.30.−v, 71.35.Gg

I. INTRODUCTION

The dynamics of a single spin in a magnetic field, B_0, under a resonantly driven excitation is described by a standard Hamiltonian,

$$\hat{H}_{\boldsymbol{\sigma}} = \gamma B_0 \hat{\sigma}_z + \gamma B_1 (\hat{\sigma}_+ e^{i\omega_0 t} + \hat{\sigma}_- e^{-i\omega_0 t}), \qquad (1)$$

where $\omega_0 = \gamma B_0$ is the Larmor frequency of the spin, γ is the gyromagnetic ratio, and B_1 is the amplitude of the driving field. This dynamics represents the seminal Rabi oscillations. In the course of these oscillations, the occupation, $n(t)$, of a Zeeman level which was populated at $t = 0$ oscillates as $n(t) = \cos^2(\Omega_R t/2)$, where $\Omega_R = \gamma B_1$ is the Rabi frequency. Naturally, the Fourier transform, $\mathbf{F}(s)$, of $n(t)$ is simply a δ peak at $s = \Omega_R$. In the ensemble of isolated spins this peak will be broadened due to disorder, caused, e.g., by a random hyperfine field.

If we consider a pair of weakly coupled spins, a and b (Fig. 1), it is described by the Hamiltonian $\hat{H}_{\boldsymbol{\sigma}_a} + \hat{H}_{\boldsymbol{\sigma}_b}$. Since the coupling is weak, both pair partners oscillate independently, so the Fourier spectrum of the Rabi oscillations of the pair is also a δ peak. It is very important that the latter is *not* the case when the Rabi oscillations are detected electrically by means of pulsed electrically detected electron spin resonance (pEDMR) techniques. Within this technique, the change, $\Delta\sigma(\tau)$, in the conductivity of the sample is measured upon application of a pulse of duration τ. The key idea why, despite the weak coupling, the Fourier transform of $\Delta\sigma(\tau)$ is not a single δ peak is that only those pairs for which the Rabi oscillations of the partners have a *correlated* character contribute to $\Delta\sigma(\tau)$. The simplest way to understand this correlation is the following: if, at the end of the pulse, the pair is in the singlet state, it will recombine rather than contribute to $\Delta\sigma$. The fact that a spin pair is a crucial entity for electrical detection of magnetic resonance has been appreciated since 1978.[1] The theoretical background of pEDMR based on spin pairs was developed in Ref. 2. The correlated character of the Rabi oscillations in pairs contributing to $\Delta\sigma$ results in a peculiar character of the Fourier transform $\mathbf{F}(s)$. This quantity is the subject of theoretical and experimental study reported in the present paper. As we demonstrate below, $\mathbf{F}(s)$ evolves in a nontrivial way upon increasing the driving field. This evolution is governed by the relation between Ω_R and the magnitude of disorder. We find good quantitative agreement between the theory and experimental results, which allows us to infer the magnitude of disorder from the fit of the experimental data.

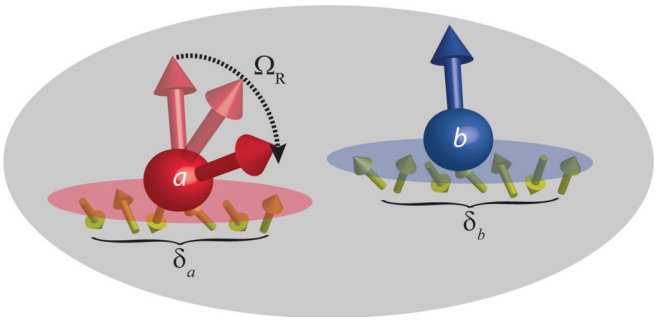

FIG. 1. (Color online) Schematic of Rabi oscillations with frequency Ω_R in a spin-$\frac{1}{2}$ pair. Components of the pair, a and b, have different environments, causing random shifts, δ_a and δ_b, from the resonant frequency, ω_0. Relevant for pEDMR are the initial and final spin configurations $|\uparrow\uparrow\rangle$ and $|\downarrow\downarrow\rangle$ only.

The paper is organized as follows. In Sec. II we discuss the context of the pEDMR spectroscopy technique in relation to the work that this study is focused on. In Sec. III, a qualitative derivation of conductivity changes, $\Delta\sigma(\tau)$, in pEDMR experiments is given which reproduces the result of rigorous consideration in Ref. 2. In Sec. IV, the analytical expression for a disorder averaged Fourier transform of $\Delta\sigma(\tau)$ is presented. In Sec. V, the theory is extended to the case where disorders for two pair partners are correlated. An analysis and

discussion of the results are given in Sec. VI. In Sec. VII, the experimental results are presented and compared to the theoretical predictions.

II. pEDMR SPECTROSCOPY ON WEAKLY COUPLED SPIN PAIRS

Over the past decade, pEDMR spectroscopy has been used increasingly for investigation of the physical nature of spin-dependent electronic transitions which influence conductivity such as excess charge carrier recombination or transport transitions through localized paramagnetic states as seen in amorphous inorganic,[3,4] crystalline,[5–8] and organic[9–13] semiconductor materials. In most of these experimental studies, pEDMR experiments are conducted within a pulse-probe scheme[14,15] where the current through the host materials of the spin systems of interest is measured while short and intensive magnetic resonant pulses are imposed. The pulsed magnetic resonant radiation prepares coherent spin noneigenstates from initial, well-defined eigenstates before the pulse. As the changed spin states will also cause changes in the spin–dependent conductivity, one can gain information about the prepared coherent spin state by integration of the electric current transient after the pulse, which eventually, on long time scales (compared to the length of the coherent excitation), will return to its prepulse steady state. The probed charge (obtained from the integrated current transient) depends on the coherent spin state after the pulse, which in turn depends on the pulse parameters (length, frequency, intensity).[14] Therefore, a measurement of the charge as a function of the applied pulse length can reveal the propagation of a spin state in the presence of the resonant radiation pulse. Thus, current detectable observations of spin-Rabi oscillations are possible.

Most EDMR-detectable spin-dependent electronic transitions reported in the literature are due to Pauli–blockade effects which occur for transitions between two paramagnetic states with $S = \frac{1}{2}$. These systems, illustrated in Fig. 1, usually require weak spin-orbit coupling as found in materials with low atomic order numbers (this means silicon and carbon materials) as well as sufficiently weak spin-spin coupling (which means exchange and dipolar interaction) within the formed pairs. In order to allow one of the electrons within this pair of paramagnetic states to undergo a transition into the other paramagnetic state (thereby forming a singlet spin manifold due to the Pauli exclusion principle), the spin pair state $|\psi\rangle$ before the transition requires non-negligible singlet content ($\langle\psi|S\rangle \neq 0$) for the transition to have a non-negligible probability. The special nature of such intermediate-pair controlled spin-dependent transition rates was first recognized by Kaplan, Solomon, and Mott,[1] who explained the magnitude of continuous-wave EDMR experiments at the time. With the advent of pEDMR about a decade ago, this model also became most significant for the understanding of many of the EDMR-detected coherent spin motion experiments.

When pEDMR is applied to the intermediate-pair processes described by Kaplan *et al.*, the observable applied to the spin ensemble is permutation symmetry (the singlet operator); it is not the magnetic polarization of the spin ensemble as is the case for conventional magnetic resonance spectroscopies, which are based on the detection of radiation. Some implications of this observable change have been discussed theoretically in previous studies on intermediate pairs for cases of no intrapair interactions,[14,16] cases of weak but non-negligible exchange interaction[17] (weak here means that the exchange interaction is much smaller than the spin-Zeeman splitting of the pair partners but not necessarily weaker than the difference of the pair partners' Larmor frequencies), and cases where disorder within the spin ensemble[18] is significant. These numerical studies have shown that an electrically detectable spin-Rabi oscillation can contain various harmonic components which can essentially form a "fingerprint" for the spin Hamiltonian of the observed pairs. Thus, conducting a Fourier analysis of an observed spin-Rabi signal (one could call this Rabi spectroscopy) can give microscopic information on the nature of charge carrier states or of paramagnetic defects.

Most of the previously published pEDMR studies have been conducted as Rabi spectroscopy experiments.[4,6,9,10,12,13] For most of these experimental data, a correct interpretation would be impossible without the information provided by the existing theoretical studies.[14,16–18] Nevertheless, these studies can only provide limited support for an experimental analysis since numerical simulations can only provide answers about the behavior of a simulated system for a fixed set of parameters; they do not reveal analytical expressions that can be fit or directly compared to experimental data, and most importantly, they oftentimes do not enhance the qualitative understanding of a simulated system. It has been the goal of this study to overcome this problem by finding a closed analytical form for the description of spin-Rabi oscillation controlled spin-dependent transition rates within spin pairs with $S = \frac{1}{2}$. The expressions derived in the following reveal the dependence of all harmonic components found with electrically, and similarly, with intermediate spin-pair-controlled optically detected transition rates on the parameters of both, the observed physical system as well as the performed Rabi-oscillation experiment.

The parameters characterizing the observed spin pair are given by the spin-orbit-controlled respective g factors for each pair partner as well as local and hyperfine fields, which in general are different for the two pair partners as well. For our purposes, all these parameters can be taken into account by the difference δ of the pair partners' Larmor frequencies. Taking this into account, we anticipate from the previously reported numerical simulations[14,16] that in the weak-driving regime where $\Omega_R \ll \delta$, the Fourier transformation $\mathbf{F}(s)$ of a Rabi oscillation transient exhibits only one peak at $s = \Omega_R$, while in the strong-driving regime ($\Omega_R \gg \delta$) there is one peak at $s = 2\Omega_R$ and no peak at $s = \Omega_R$. The crossover between these two situations occurs around $\Omega_R \approx \delta$.

This crossover with increasing Ω_R was demonstrated experimentally for spin-dependent polaron pair recombination processes in different organic semiconductor materials.[12,13] Currently, it is rather difficult (if not impossible) to extract quantitative information from such experimentally measured Rabi spectra $\mathbf{F}(s)$ due to the lack of theoretical predictions. On the other hand, the theoretical problem is well posed. When the exchange and dipolar coupling strength within a pair are smaller than δ_0 (which we assume), the shape of the Fourier transform depends on only two parameters: δ_0, which is the r.m.s. value of δ; and Ω_R.

In the following, the Fourier components of the Rabi spectrum $\mathbf{F}(s)$ are calculated analytically. We find that the width of the crossover region is broad and extends from $\frac{\Omega_R}{\delta_0} \approx 0.3$, where the $s = 2\Omega_R$ peak appears, to $\frac{\Omega_R}{\delta_0} \approx 2$, where it dominates over the $s = \Omega_R$ peak. Most importantly, the analytical treatment reveals that $\mathbf{F}(s)$ consists not of just two peaks (as discussed in most experimental studies) but, rather, of *three* peaks. The origin of the third peak, which occurs at frequencies $s \ll \Omega_R$, is due to a disorder-induced distribution of δ, which implies that even at strong Ω_R, the two spins in the pair do not precess entirely in phase. This third peak is harder to observe experimentally compared to the two with higher frequencies, yet a prediction of its shape and evolution with Ω_R is provided. Also, a correlation study of disorder within pairs affects the shape of an ensemble average of $\mathbf{F}(s)$. This follows from a previous numerical study of the ratio between the magnitudes of the $s = \Omega_R$ and $s = 2\Omega_R$ Rabi oscillation peaks,[18] which was conducted for particular value sets of δ_0 and Ω_R.

III. DEPENDENCE OF pEDMR-INDUCED CONDUCTIVITY CHANGES ON THE PULSE DURATION τ

The pair partners within a spin pair are denoted a and b, respectively. Before a pulse is applied to a spin pair, it will rest in one of its four spin eigenstates, as both a and b can be either in a $|\downarrow\rangle$ or in a $|\uparrow\rangle$ state. The important qualitative observation made in Ref. 2 is that only initial configurations $|\downarrow\downarrow\rangle$ and $|\uparrow\uparrow\rangle$ of the pair exist, as the other two eigenstates with singlet content are very short-lived. The $|\downarrow\downarrow\rangle$ and $|\uparrow\uparrow\rangle$ states are therefore responsible for the change in conductivity after the end of the pulse. Without confinement of generality, one can assume that at $t = 0$ both a and b are in the $|\downarrow\rangle$ state. The respective populations of the $|\downarrow\rangle$ states will then evolve according to the Rabi formula,

$$n_{a,b}(t) = 1 - \frac{\Omega_R^2}{\Omega_R^2 + \delta_{a,b}^2} \sin^2 \sqrt{\frac{1}{4}\left(\Omega_R^2 + \delta_{a,b}^2\right)} t, \qquad (2)$$

where $\delta_a = \omega_a - \omega$ and $\delta_b = \omega_b - \omega$ are the detuning frequencies of a and b, respectively. A detuning frequency is the difference between a Larmor frequency ω_a or ω_b and the frequency ω of the driving field. After the pulse ends at $t = \tau$ the pair is in the $|\downarrow\downarrow\rangle$ state with probability $P_{\downarrow\downarrow} = n_a(\tau)n_b(\tau)$ and in the $|\uparrow\uparrow\rangle$ state with probability $P_{\uparrow\uparrow} = (1 - n_a(\tau))(1 - n_b(\tau))$. Then the probability of finding the pair in one of the states $|\downarrow\downarrow\rangle$ or $|\uparrow\uparrow\rangle$ is equal to

$$\begin{aligned} P(\tau) &= P_{\uparrow\uparrow} + P_{\downarrow\downarrow} \\ &= 1 - n_a(\tau) - n_b(\tau) + 2n_a(\tau)n_b(\tau). \end{aligned} \qquad (3)$$

It is easy to see that Eq. (3) also applies when the pair is initially in the $|\uparrow\uparrow\rangle$ state. Equation (3) coincides with the corresponding expression for the τ-dependent part of the diagonal elements of the density matrix of the pair derived in Ref. 14. The probability $P(\tau)$ serves as the initial condition for the transient restoration of the steady-state current after the pulse.[14] Thus, $\Delta\sigma$ can be identified with $P(\tau)$ within a factor. An expression for $\Delta\sigma(\tau)$ averaged over the contributions from all pairs within a pair ensemble is then obtained from

$$\langle \Delta\sigma(\tau) \rangle = \frac{1}{2\pi\delta_0^2} \int d\delta_a d\delta_b \exp\left[-\frac{\delta_a^2 + \delta_b^2}{2\delta_0^2}\right] \Delta\sigma(\delta_a, \delta_b, \tau). \qquad (4)$$

Note that this expression for $\langle \Delta\sigma(\tau) \rangle$ can also be written as

$$\langle \Delta\sigma(\tau) \rangle = 1 - 2T(\tau) + 2T^2(\tau), \qquad (5)$$

where the function $T(\tau)$ is defined as

$$\begin{aligned} T(\tau) = \frac{1}{\sqrt{2\pi}\delta_0} \int d\delta\, e^{-\delta^2/2\delta_0^2} \left(\frac{\Omega_R^2}{\Omega_R^2 + \delta^2}\right) \\ \times \sin^2 \sqrt{\frac{1}{4}\left(\Omega_R^2 + \delta^2\right)}\, \tau. \end{aligned} \qquad (6)$$

In the limit of long pulses, $T(\tau)$ approaches a constant in an oscillatory fashion; the amplitude of the oscillations falls off slowly, as $\tau^{-1/2}$, with the length of the pulse.[19] For strong disorder ($\delta \gg \Omega_R$) the derivative can be expressed through the zero-order Bessel function[10] $T'(\tau) = 2^{-3/2}\pi^{1/2}\Omega_R^3\delta_0^{-1}J_0(\Omega_R\tau)$.

While the second term in Eq. (5) describes Rabi oscillations within either component a or component b of the pair, the third term "knows" about the collective spin precession of a and b. However, the T^2 term also contains contributions from the individual precessions of pair partners a and b. We therefore subtract these contributions and group them with the T term in Eq. (5) prior to performing the Fourier transform. By substituting Eqs. (2) into (3), we get

$$\begin{aligned} \Delta\sigma(\tau) = \frac{1}{2} + \frac{\delta_a^2\delta_b^2}{2\left(\Omega_R^2 + \delta_a^2\right)\left(\Omega_R^2 + \delta_b^2\right)} + [G_1(\delta_a, \delta_b, \tau) \\ + G_1(\delta_b, \delta_a, \tau)] + G_-(\delta_a, \delta_b, \tau) + G_+(\delta_a, \delta_b, \tau), \end{aligned} \qquad (7)$$

where the functions describing the three harmonic Rabi-oscillation peaks are defined as

$$G_1(\delta_a, \delta_b, \tau) = \frac{\Omega_R^2\delta_b^2}{2}\left[\frac{\cos\left(\sqrt{\Omega_R^2 + \delta_a^2}\,\tau\right)}{\left(\Omega_R^2 + \delta_a^2\right)\left(\Omega_R^2 + \delta_b^2\right)}\right], \qquad (8)$$

$$G_-(\delta_a, \delta_b, \tau) = \frac{\Omega_R^4}{4}\left[\frac{\cos\left\{\left(\sqrt{\Omega_R^2 + \delta_a^2} - \sqrt{\Omega_R^2 + \delta_b^2}\right)\tau\right\}}{\left(\Omega_R^2 + \delta_a^2\right)\left(\Omega_R^2 + \delta_b^2\right)}\right], \qquad (9)$$

$$G_+(\delta_a, \delta_b, \tau) = \frac{\Omega_R^4}{4}\left[\frac{\cos\left\{\left(\sqrt{\Omega_R^2 + \delta_a^2} + \sqrt{\Omega_R^2 + \delta_b^2}\right)\tau\right\}}{\left(\Omega_R^2 + \delta_a^2\right)\left(\Omega_R^2 + \delta_b^2\right)}\right]. \qquad (10)$$

The above terms G_1, G_+, and G_- describe the peaks $s = \Omega_R$, $s = 2\Omega_R$, and $s \ll \Omega_R$, contained in the Fourier transform $\mathbf{F}(s)$, respectively.

IV. AVERAGING OVER DISORDER WITHIN A SPIN PAIR ENSEMBLE

Variations of the magnetic resonance frequency of each pair partner in each individual pair can occur due to (i) variations in the spin-orbit coupling, which change the g factor.[20] This is

seen in disordered materials, where the lengths and angles of chemical bonds can vary strongly.[3,4] Variations can also occur due to (ii) random hyperfine fields, which can strongly fluctuate throughout a material because of the small polarization nuclear spins even at low temperature and high magnetic fields.[12,21] We define the Fourier spectrum of the conductivity change from the steady state as

$$\mathbf{F}(s) = \int_0^\infty d\tau \cos(s\tau)\langle(\Delta\sigma(\tau) - \Delta\sigma(0))\rangle. \tag{11}$$

The expression can be decomposed into three contributions—$\mathbf{F}(s) = \mathbf{F}_1(s) + \mathbf{F}_0(s) + \mathbf{F}_2(s)$—which derive from the terms G_1, G_-, and G_+ terms in Eq. (7). Obviously, the time integration of each term yields a δ function.

Our task is to perform the averaging of each δ function over disorder, as in Eq. (4). We start from $\mathbf{F}_1(s)$, which describes a peak near $s = \Omega_R$. For this contribution, the averaging over δ_a, δ_b reduces to the product of averages:

$$\mathbf{F}_1(s) = \frac{\Omega_R^2}{8\delta_0^2}\int d\delta_a\, e^{-\delta_a^2/2\delta_0^2}\left[\frac{\delta\left(s-\sqrt{\Omega_R^2+\delta_a^2}\right)}{\Omega_R^2+\delta_a^2}\right] \times \int d\delta_b\, e^{-\delta_b^2/\delta_0^2}\left(\frac{\delta_b^2}{\Omega_R^2+\delta_b^2}\right). \tag{12}$$

It is convenient to evaluate the integral over δ_a with the help of the δ function. The second integral can be reduced to the error function, leading to

$$\mathbf{F}_1(s) = \left(\frac{\Omega_R^3}{4\delta_0^2 s\sqrt{s^2-\Omega_R^2}}\right)\exp\left[-\frac{s^2-\Omega_R^2}{2\delta_0^2}\right] f\left(\frac{\Omega_R^2}{2\delta_0^2}\right), \tag{13}$$

where the function f is defined as

$$f(b) = \int_{-\infty}^{\infty} dy\, e^{-y^2 b}\left(\frac{y^2}{1+y^2}\right) = \sqrt{\pi}\left[\frac{1}{b^{1/2}} - \sqrt{\pi}e^b\ \mathrm{erfc}(\sqrt{b})\right]. \tag{14}$$

For $\mathbf{F}_2(s)$, it is convenient, after substituting (10) into (11), to perform an integration over δ_a, δ_b in polar coordinates. Upon introducing the new variables

$$\delta_a = \sqrt{2}v\cos\phi, \quad \delta_b = \sqrt{2}v\sin\phi, \tag{15}$$

the expression for $\mathbf{F}_2(s)$ acquires the form

$$\mathbf{F}_2(s) = \frac{\Omega_R^4}{8\delta_0^2}\int_0^\infty dv\, v\, e^{-v^2/\delta_0^2}\int_0^{2\pi} d\phi \times \frac{\delta\left(s-\sqrt{\Omega_R^2+2v^2\cos^2\phi}-\sqrt{\Omega_R^2+2v^2\sin^2\phi}\right)}{\left(\Omega_R^2+2v^2\cos^2\phi\right)\left(\Omega_R^2+2v^2\sin^2\phi\right)}. \tag{16}$$

Without the denominator, it is straightforward to perform an integration over ϕ, which yields

$$\int_0^{2\pi} d\phi\,\delta\left(s-\sqrt{\Omega_R^2+2v^2\cos^2\phi}-\sqrt{\Omega_R^2+2v^2\sin^2\phi}\right) = \frac{2\left|2\Omega_R^2+2v^2-s^2\right|}{\sqrt{\left[\left(\frac{s^2}{2}-v^2\right)^2-\Omega_R^2 s^2\right]\left[\left(\Omega_R^2+v^2\right)-\frac{s^2}{4}\right]}}. \tag{17}$$

With the denominator, Eq. (17) is to be divided by the value $\frac{1}{4}(s^2-2\Omega_R^2-2v^2)^2$ of the denominator, where the argument of the δ function is 0, which yields

$$\mathbf{F}_2(s) = \frac{\Omega_R^4}{\delta_0^2}\int_0^{\sqrt{\frac{s^2}{2}-s\Omega_R}} \frac{dv\, v\, e^{-v^2/\delta_0^2}}{\left|s^2-2\Omega_R^2-2v^2\right|} \times \frac{1}{\sqrt{\left[\left(\frac{s^2}{2}-v^2\right)^2-\Omega_R^2 s^2\right]\left[\left(\Omega_R^2+v^2\right)-\frac{s^2}{4}\right]}}. \tag{18}$$

Equation (18) is defined only for $s > 2\Omega_R$. As s approaches $2\Omega_R$, both brackets under the square root turn to 0. At the same time, the integration interval also shrinks to 0. However, the factor $|s^2-2\Omega_R^2-2v^2|$ in the denominator is nonsingular near $s = 2\Omega_R$. To illuminate the behavior of $\mathbf{F}_2(s)$ near the threshold, it is convenient to make the substitution $w = v^2 - \frac{s^2}{4} + \Omega_R^2$ in the integral of Eq. (18). It then assumes the form

$$\mathbf{F}_2(s) = \left(\frac{\Omega_R^4}{2\delta_0^2}\right)e^{-\frac{\frac{s^2}{4}-\Omega_R^2}{\delta_0^2}}\int_0^{\left(\frac{s}{2}-\Omega_R\right)^2} \frac{dw\, e^{-w/\delta_0^2}}{\sqrt{w\left[\left(\frac{s}{2}-\Omega_R\right)^2-w\right]}} \times \frac{1}{\left|\frac{s^2}{2}-2w\right|\sqrt{\left[\left(\frac{s}{2}+\Omega_R\right)^2-w\right]}}. \tag{19}$$

Now we see that only the first two factors in the denominator are singular when s is close to $2\Omega_R$, where the $s = 2\Omega_R$ peak occurs. In this domain we can set $w = 0$ in the last two factors and take them out of the integrand. Then the remaining integral readily reduces to the modified Bessel function, $I_0(y)$, and we get

$$\mathbf{F}_2(s) = \left(\frac{2\Omega_R^4}{\delta_0^2 s^2}\right)\left(\frac{e^{-\frac{s^2/4-\Omega_R^2}{\delta_0^2}}}{s+2\Omega_R}\right)G\left[\frac{(s-2\Omega_R)^2}{4\delta_0^2}\right], \tag{20}$$

where

$$G(b) = \int_0^b \frac{dx\ e^{-x}}{\sqrt{x(b-x)}} = \pi e^{-b/2}\ I_0\left(\frac{b}{2}\right). \tag{21}$$

The analysis of the shape of the $s = 2\Omega_R$ peak, given in Sec. V, reveals that the approximation in Eq. (20) describes not only the vicinity $(s-2\Omega_R) \ll \Omega_R$ but the entire peak when Ω_R is bigger than $0.3\delta_0$.

Finally, we turn our attention to the peak at $s \ll \Omega_R$. The initial expression for $\mathbf{F}_2(s)$ differs from Eq. (16) for $\mathbf{F}_0(s)$ in only one respect. Instead of the sum, $\sqrt{\Omega_R^2+\delta_a^2}+\sqrt{\Omega_R^2+\delta_a^2}$, in the argument of the δ function it contains a difference, $\sqrt{\Omega_R^2+\delta_a^2}-\sqrt{\Omega_R^2+\delta_a^2}$. The angular integration in polar

coordinates is therefore performed in a similar way as Eq. (17):

$$\int_0^{2\pi} d\phi\, \delta\Big(s - \sqrt{\Omega_R^2 + 2v^2\cos^2\phi} + \sqrt{\Omega_R^2 + 2v^2\sin^2\phi}\Big) = \frac{\left|2\Omega_R^2 + 2v^2 - s^2\right|}{\sqrt{\left[\left(\frac{s^2}{2} - v^2\right)^2 - \Omega_R^2 s^2\right]\left[\left(\Omega_R^2 + v^2\right) - \frac{s^2}{4}\right]}}. \quad (22)$$

Note that, compared to Eq. (22), the integral in Eq. (17) has an extra factor of 2. This is because the argument of the δ function in Eq. (22) turns to 0 at two values of ϕ, while in Eq. (17), it turns to 0 at four values of ϕ. To get the final expression for $\mathbf{F}_0$ one again has to divide Eq. (22) by the value of the denominator at the zero points of the δ function, which is equal to $\frac{1}{4}(s^2 - 2\Omega_R^2 - 2v^2)^2$, i.e., the same as in $\mathbf{F}_2(s)$. This leads to

$$\mathbf{F}_0(s) = \frac{\Omega_R^4}{2\delta_0^2}\int_{\sqrt{\frac{s^2}{2}+s\Omega_R}}^{\infty} \frac{dv\, v\, e^{-v^2/\delta_0^2}}{\sqrt{\left(\frac{s^2}{2} - v^2\right)^2 - \Omega_R^2 s^2}} \times \frac{1}{\left|s^2 - 2\Omega_R^2 - 2v^2\right|\sqrt{\left(\Omega_R^2 + v^2\right) - \frac{s^2}{4}}}. \quad (23)$$

We see again that only the first factor in the denominator is singular at the lower limit $v = (\frac{s^2}{2} + s\Omega_R)^{1/2}$. Thus, for small s, the peak is described by substituting $s = 0$ into the second and third factors in the denominator, which leads to

$$\mathbf{F}_0(s) = \frac{\Omega_R}{4\delta_0^2}\int_{\sqrt{\frac{s^2}{2}+s\Omega_R}}^{\infty} \frac{dv\, v\, e^{-v^2/\delta_0^2}}{\sqrt{\left(\frac{s^2}{2} - v^2\right)^2 - \Omega_R^2 s^2}}. \quad (24)$$

The remaining integral can be expressed via the Macdonald function, $K_0(y)$, which yields

$$\mathbf{F}_0(s) = \left(\frac{\Omega_R}{8\delta_0^2}\right) e^{-s^2/2\delta_0^2} K_0\left(\frac{s\Omega_R}{\delta_0^2}\right). \quad (25)$$

We see in Sec. V that the expression in Eq. (25) describes the entire peak when Ω_R is big enough: $\Omega_R \gtrsim \delta_0$.

V. CORRELATION BETWEEN THE PAIR PARTNER DISORDER

Due to the proximity of the pair partners in each pair, the disorder-related randomness of δ_a and δ_b may be correlated. Examples of such a correlation are the common exposure of the polaronic state in organic semiconductors to an overlapping nuclear spin bath and the correlation of the spin-orbit interaction in a disordered semiconductor due to local strain fields.[22] In such cases, δ_a and δ_b are not statistically independent and the degree of overlap can be expressed by a correlation parameter, x $(0 < x < 1)$. Then the joint distribution function of δ_a, δ_b assumes the form

$$\Phi(\delta_a,\delta_b) = \frac{1}{2\pi\delta_0^2\sqrt{1-x^2}}\exp\left[-\frac{\delta_a^2 + \delta_b^2 - 2x\delta_a\delta_b}{2\delta_0^2(1-x^2)}\right]. \quad (26)$$

We study the effect of correlation for the limit $\Omega_R \gg \delta_0$ when all three peaks are well developed and do not overlap. In this limit, we can use the expansion $\sqrt{\Omega_R^2 + \delta_{a,b}^2} \approx \Omega_R + \frac{\delta_{a,b}^2}{2\Omega_R}$ in the arguments of the δ functions. We can also replace $\sqrt{\Omega_R^2 + \delta_{a,b}^2}$ with Ω_R in the denominators of Eqs. (8) to (10).

With these simplifications the expression for $\mathbf{F}_1(s)$ assumes the form

$$\mathbf{F}_1(s) = \frac{1}{8\delta_0^2\Omega_R^2\sqrt{1-x^2}}\int d\delta_b \int d\delta_a\, \delta_b^2 \times \exp\left[-\frac{\delta_a^2 + \delta_b^2 - 2x\delta_b\delta_a}{2\delta_0^2(1-x^2)}\right]\delta\left(s - \Omega_R - \frac{\delta_a^2}{2\Omega_R}\right). \quad (27)$$

Integrating over δ_a with the help of the δ function yields

$$\mathbf{F}_1(s) = \frac{\exp\left[-\frac{\Omega_R(s-\Omega_R)}{\delta_0^2(1-x^2)}\right]}{\left(4\Omega_R\delta_0^2\sqrt{1-x^2}\right)\sqrt{2\Omega_R(s-\Omega_R)}} \times \int d\delta_b \delta_b^2 \exp\left[-\frac{\delta_b^2}{2\delta_0^2(1-x^2)}\right] \times \cosh\left(\frac{\delta_b x\sqrt{2\Omega_R(s-\Omega_R)}}{\delta_0^2(1-x^2)}\right). \quad (28)$$

Subsequent integration over δ_b is straightforward, leading to

$$\mathbf{F}_1(s) = \frac{\sqrt{\pi}\delta_0(1-x^2)}{4\Omega_R\sqrt{\Omega_R(s-\Omega_R)}}\left[1 + \frac{2x^2\Omega_R(s-\Omega_R)}{\delta_0^2(1-x^2)}\right] \times \exp\left[-\frac{\Omega_R(s-\Omega_R)}{\delta_0^2}\right]. \quad (29)$$

We see that the correlation parameter, x, enters this expression only in the prefactor. In the limit of $x \to 0$, Eq. (29) matches Eq. (13), as can be seen when $\Omega_R \gg \delta_0$ is assumed and Eq. (13) is expanded around $s = \Omega_R$.

In the limit of large Ω_R the definition of $\mathbf{F}_2(s)$ becomes

$$\mathbf{F}_2(s) = \left(\frac{1}{16\delta_0^2\sqrt{1-x^2}}\right)\int d\delta_a\, d\delta_b \times \exp\left[-\frac{\delta_a^2 + \delta_b^2 - 2x\delta_b\delta_a}{2\delta_0^2(1-x^2)}\right]\delta\left(s - 2\Omega_R - \frac{\delta_a^2 + \delta_b^2}{2\Omega_R}\right). \quad (30)$$

Both integrals over δ_a and δ_b can be taken explicitly upon the introduction of polar coordinates,

$$r = \sqrt{2\left(\delta_a^2 + \delta_b^2\right)}, \quad \phi = \arctan\left(\frac{\delta_a - \delta_b}{\delta_a + \delta_b}\right), \quad (31)$$

so that Eq. (30) assumes the form

$$\mathbf{F}_2(s) = \left(\frac{1}{32\delta_0^2\sqrt{1-x^2}}\right)\int dr\, r\, d\phi \times \exp\left[-\frac{r^2(1 + x\cos 2\phi)}{4\delta_0^2(1-x^2)}\right]\delta\left(s - 2\Omega_R - \frac{r^2}{4\Omega_R}\right). \quad (32)$$

After integrating over r by using the δ function, the remaining integral over ϕ reduces to $I_0(y)$, and we arrive at

$$\mathbf{F}_2(s) = \left(\frac{\pi\Omega_R}{8\delta_0^2\sqrt{1-x^2}}\right)\exp\left[-\frac{\Omega_R(s-2\Omega_R)}{\delta_0^2(1-x^2)}\right] \times I_0\left[\frac{\Omega_R x(s-2\Omega_R)}{\delta_0^2(1-x^2)}\right]. \quad (33)$$

Similarly to the noncorrelated case, $\mathbf{F}_2(s)$ is expressed through $I_0(y)$. However, note that the argument of $I_0(y)$ in Eq. (33) is completely different from Eq. (20). In fact, Eq. (33) was derived for the case where $I_0(\frac{b}{2})$ in Eq. (21) should be replaced by 1.

In the presence of a disorder correlation, the shape of $\mathbf{F}_0(s)$ can also be expressed via the Macdonald function with an x-dependent argument. To see this, we take the definition

$$\mathbf{F}_0(s) = \left(\frac{1}{16\delta_0^2\sqrt{1-x^2}}\right)\int d\delta_a d\delta_b \times \exp\left[-\frac{\delta_a^2+\delta_b^2-2x\delta_b\delta_a}{2\delta_0^2(1-x^2)}\right]\delta\left(s-\frac{\delta_a^2-\delta_b^2}{2\Omega_R}\right) \tag{34}$$

and introduce polar coordinates,

$$r = \sqrt{\frac{\delta_a^2+\delta_b^2-2x\delta_b\delta_a}{2\delta_0^2(1-x^2)}},$$
$$\phi = \arctan\left[\sqrt{\frac{1+x}{1-x}}\left(\frac{\delta_a-\delta_b}{\delta_a+\delta_b}\right)\right]. \tag{35}$$

Equation (34) then becomes

$$\mathbf{F}_0(s) = \frac{1}{8}\int dr\, r\, e^{-r^2}\int d\phi\,\delta\left(s-\frac{\delta_0^2 r^2\sqrt{1-x^2}}{\Omega_R}\sin 2\phi\right). \tag{36}$$

The integration over ϕ can be done explicitly by using the δ function, yielding

$$\mathbf{F}_0(s) = \frac{1}{4s}\int_{\left(\frac{s\Omega_R}{\delta_0^2\sqrt{1-x^2}}\right)^{1/2}}^{\infty}\frac{dr\, r\, e^{-r^2}}{\sqrt{\frac{\delta_0^4(1-x^2)}{\Omega_R^2 s^2}r^4-1}}. \tag{37}$$

The reduction to the Macdonald function can then be achieved by the substitution $r^2 = \frac{s\Omega_R}{\delta_0^2\sqrt{1-x^2}}r_1$, which reveals

$$\mathbf{F}_0(s) = \left(\frac{\Omega_R}{8\delta_0^2\sqrt{1-x^2}}\right)K_0\left[\frac{s\Omega_R}{\delta_0^2\sqrt{1-x^2}}\right]. \tag{38}$$

VI. ANALYSIS AND DISCUSSION

The most important results of this study are the analytical expressions for the line shapes of Rabi-oscillation peaks as they can be found in the Fourier analysis (the Rabi spectra) of the pulse-length-dependent conductivity changes $\Delta\sigma(\tau)$ that are measured with pEDMR experiments. For the case of uncorrelated disorder, Eqs. (13), (20), and (25) reveal these peak shapes for the oscillation peaks $\mathbf{F}_1(s)$, $\mathbf{F}_0(s)$, and $\mathbf{F}_2(s)$, respectively. For the case of correlated disorder, the same peaks are described by Eqs. (29), (33), and (38). We consider now the limit $\Omega_R \gg \delta_0$, when all three peaks are well developed. It is easy to see that, for uncorrelated disorder, all three peaks exhibit the same exponential tail,

$$\mathbf{F}_1(s) \approx \frac{\pi^{1/2}}{4\Omega_R}\sqrt{\frac{\Delta s}{s-\Omega_R}}e^{-\frac{s-\Omega_R}{\Delta s}},$$
$$\mathbf{F}_0(s) \approx \frac{\sqrt{\pi}}{8\sqrt{2s\Delta s}}e^{-\frac{s}{\Delta s}}, \quad \mathbf{F}_2(s) \approx \frac{\pi}{8\Delta s}e^{-\frac{s-2\Omega_R}{\Delta s}}, \tag{39}$$

where the characteristic width of the tail is given by

$$\Delta s = \frac{\delta_0^2}{\Omega_R}. \tag{40}$$

Naturally, all three peaks shrink with increasing Ω_R. It is less trivial to realize that, for the same deviation from the origin, the peaks $\mathbf{F}_0$ and $\mathbf{F}_2$ have a larger magnitude than $\mathbf{F}_1$, whose terms contain $\Omega_R \gg \Delta s$ in the denominator. This relation between the peaks is illustrated in Fig. 2(c).

We consider now the opposite limit of strong but uncorrelated disorder where $\delta_0 \gg \Omega_R$ and $x = 0$. Equation (20) implies that $\mathbf{F}_2(2\Omega_R) = \frac{\Omega_R}{16\delta_0^2}$ is always finite at its peak. At

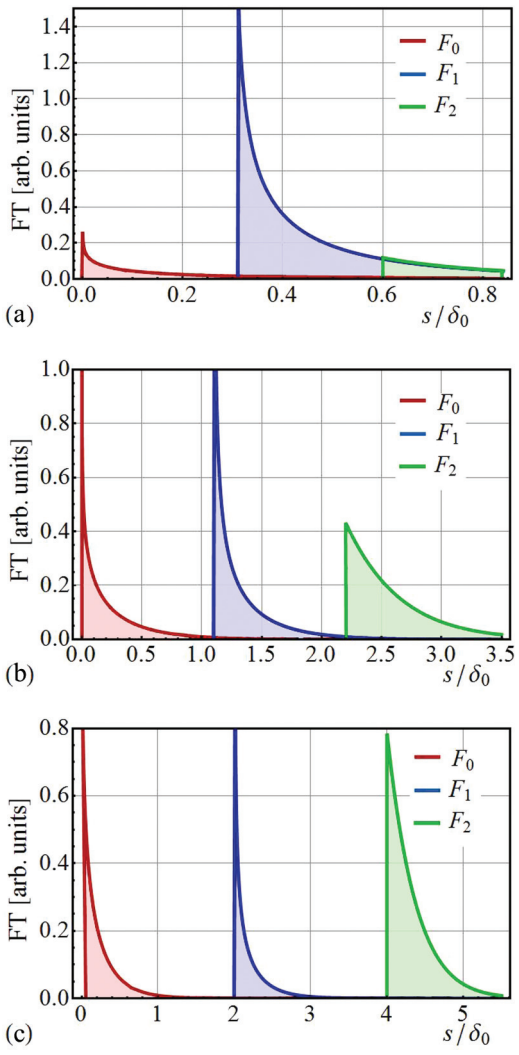

FIG. 2. (Color online) The shapes of the three peaks $s \ll \Omega_R$ (left; red), $s = \Omega_R$ (center; blue), and $s = 2\Omega_R$ (right; green) in the Fourier transform of $\Delta\sigma(\tau)$ are plotted for three values of the dimensionless Rabi frequency $w = \Omega_R/\delta_0$: (a) $w = 0.3$, (b) $w = 1.1$, and (c) $w = 2$.

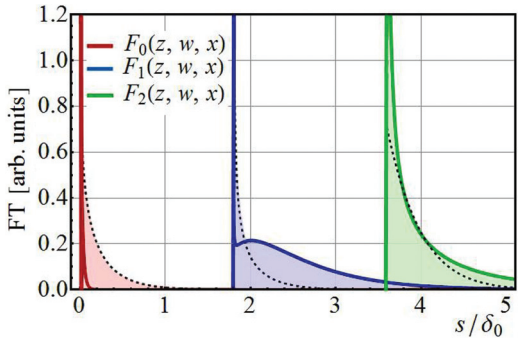

FIG. 3. (Color online) Illustration of the effect of an intrapair correlation of disorder on the shapes of the three peaks, $s \ll \Omega_R$ (left; red), $s = \Omega_R$ (center; blue), and $s = 2\Omega_R$ (right; green), in the Fourier transform of $\Delta\sigma(\tau)$. Dashed lines correspond to uncorrelated disorder ($x = 0$), while solid lines correspond to strongly correlated disorder ($x = 0.95$). The dimensionless Rabi frequency is $w = \Omega_R/\delta_0 = 1.8$.

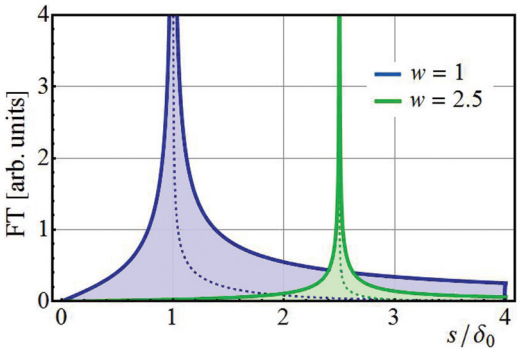

FIG. 4. (Color online) Solid lines: Fourier transform of the central peak plotted using the definition $[\mathbf{F}^2(s) + \tilde{\mathbf{F}}^2(s)]^{1/2}$ from Eqs. (11) and (41) for two values of the dimensionless Rabi frequency $w = \Omega_R/\delta_0$. Dashed lines show the corresponding Fourier transform plotted using $\mathbf{F}(s)$ only.

the same time, the value of $\mathbf{F}_1(s)$ at $s = 2\Omega_R$ is $\frac{\pi^{3/2}}{4\sqrt{6}\delta_0}$; i.e., it is bigger than $\mathbf{F}_2(2\Omega_R)$. Therefore, the $s = 2\Omega_R$ peak is indistinguishable on the background of the $s = \Omega_R$ peak. This behavior reflects the physics of the weak-driving regime,[14] where only one component of the pair can be in resonance with the driving field at any time. Numerically, however, the $s = 2\Omega_R$ peak is already pronounced at $\Omega_R > 0.3\delta_0$, as shown in Fig. 2(a). For the given strength of Ω_R, the approximation, Eq. (20), using the modified Bessel function is already justified.

The low-frequency Rabi-oscillation peak which is described by Eq. (25) diverges logarithmically in the limit of $s \to 0$ when $\mathbf{F}_0(s) \propto \ln(1/s)$. Nevertheless, the peak still loses to $\mathbf{F}_1(s)$ in the weak-driving regime due to its small prefactor, $\frac{\Omega_R}{8\delta_0^2}$. The line shape of this peak is described by Eq. (25) when the ratio Ω_R/δ_0 exceeds 1. This could be the reason why this peak has not received much attention in previous experimental studies since this regime is hard (yet not impossible) to attain experimentally.

Figure 3 illustrates how the intrapair correlation of disorder affects the shapes of the peaks in the strong-driving regime. One can see that the prime effect of the correlation is a dramatic narrowing of the low-frequency peak. This narrowing reflects the fact that the low-frequency peak is entirely due to inequivalences of the pair partners, which are suppressed by the correlation. Another effect of strong correlation is that $\mathbf{F}_1(s)$ develops a maximum at $(s - \Omega_R) = \Delta s/2$ and a minimum at $(s - \Omega_R) = (1 - x)\Delta s$. The origin of the maximum is that, for a full correlation ($x = 1$), the portion of resonant pairs in which only one partner participates in the Rabi oscillations vanishes. More precisely, $\mathbf{F}_1(s) \propto (s - \Omega_R)^{1/2} \exp[-\frac{s-\Omega_R}{\Delta s}]$ at $x = 1$, giving rise to a maximum. For a small but finite $(1 - x)$ such pairs exist and cause "normal" divergent behavior, $\mathbf{F}_1(s) \propto \frac{1-x}{\sqrt{s-\Omega_R}}$ at $s \to \Omega_R$, resulting in a minimum. Finally, the $s = 2\Omega_R$ peak becomes enhanced by a correlation near the origin for the same reason that $\mathbf{F}_1(s)$ gets depleted. Conservation of the total area, which applies for all three peaks, is achieved due to depletion in the body.

We note that disorder broadens the peaks in $\mathbf{F}(s)$ only to the right (higher frequencies) from corresponding thresholds. This is due to the adopted definition [Eq. (11)] of the Fourier transform. If we use the standard definition, $[\mathbf{F}^2(s) + \tilde{\mathbf{F}}^2(s)]^{1/2}$, where $\tilde{\mathbf{F}}(s)$ is defined as

$$\tilde{\mathbf{F}}(s) = \int_0^\infty d\tau \sin(s\tau)\langle(\Delta\sigma(\tau) - \Delta\sigma(0))\rangle, \qquad (41)$$

the disorder will broaden the peaks both to the left and to the right (to higher and lower frequencies) from the threshold. This is illustrated in Fig. 4 for the central peak at $s = \Omega_R$. A formal expression,

$$\tilde{\mathbf{F}}_1(s) = \left(\frac{\Omega_R^3}{2\pi\delta_0^2 s}\right) \int d\delta \frac{e^{-\delta^2/2\delta_0^2}}{s^2 - \Omega_R^2 - \delta^2} f\left(\frac{\Omega_R^2}{2\delta_0^2}\right), \qquad (42)$$

emerges as an obvious modification of Eq. (13). This integral in Eq. (42) can be expressed through the error function. It is nonzero for $s < \Omega_R$ and for $s > \Omega_R$. Near $s = \Omega_R$ it diverges as $|s - \Omega_R|^{-1/2}$. As shown in Fig. 4, the inclusion of $\tilde{\mathbf{F}}(s)$ in the Fourier transform (as done for most previously published pEDMR and pulsed optically detected magnetic resonance (pODMR) Rabi spectroscopy studies) leads to a significant unnecessary increase in the peak width, which complicates the analysis of experimental data.

VII. EXPERIMENT AND COMPARISON TO THE THEORY

For an illustration of the artificial broadening effect, we refer to an experimental data set which is displayed in the inset in Fig. 5. The data show electrically detected spin-Rabi oscillation in a π-conjugated polymer diode measured at room temperature in identically prepared samples and conditions as for the experiments described in Ref. 23. The diode consisted of a device stack made of a glass substrate on which a transparent indium tin oxide (ITO) was deposited as the anode contact, followed by a layer of poly(3,4-ethylenedioxythiophene):poly(styrenesulfonate) that served as a hole injection layer, an active layer consisting of an approximately 100-nm-thick poly[2-methoxy-5-(2-ethylhexyloxy)-*p*-phenylenevinylene] (MEH-PPV) film, a calcium electron injection layer, and an aluminium top contact. MEH-PPV is a prototypical π-conjugated polymer semiconductor that, technologically, has been used for organic electronics, especially organic light-emitting diodes.

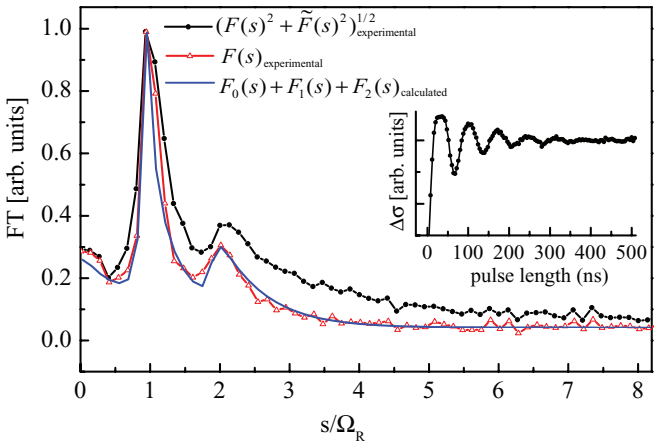

FIG. 5. (Color online) Fourier transformation of an electrically detected spin-Rabi oscillation measured in an organic polymer diode. Inset: Measured data set; for details on the measurement see the text as well as Ref. 23. The black curve displays the *absolute* Fourier transform, $\sqrt{F(s)^2+\tilde{F}(s)^2}$, of the data in the inset. The red curve displays the *real part*, $F(s)$, of the Fourier transform of the data in the inset. The blue curve represents a fit of the experimental data with the analytical function $F(s)=F_0(s)+F_1(s)+F_2(s)$.

The signal was measured by detection of changes to a forward steady-state current of $I=100\ \mu$A, under application of a 4-V bias at room temperature. The experiment was conducted under an applied magnetic field of 344 mT; the applied magnetic resonant excitation had a frequency of 9.6606 GHz and a driving-field strength $B_1=0.519(36)$ mT produced by a 27-W coherent pulsed microwave source. The inset in Fig. 5 shows the measured raw data. It displays a rapidly dephasing oscillation which is due to inhomogeneities of the applied B_1 field.[23] Figure 5 shows two Fourier transformations of the data displayed in the inset plotted on a normalized scale as a function of the frequency in units of $\Omega_R=\gamma B_1$. The black curve displays the absolute Fourier transform of the experimental data, while the red $[F(s)_{\text{experimental}}]$ curve displays the in-phase (cos) component of the Fourier transform. From these curves, it becomes evident that the absolute Fourier transform displays significant broadening of the Rabi spectrum without providing additional insight. It is noted that the peak widths of the plot in Fig. 5 are too close to the frequency resolution of the Fourier transform to unambiguously identify that the peaks of the red $[F(s)_{\text{experimental}}]$ curve are more asymmetric compared to those of the black curve. With the given length of the original data set (500 ns), an additional symmetric broadening effect that overlaps the intrinsic peak shapes is introduced to both Fourier transforms. However, for the data sets displayed in Fig. 5, one can conclude that the analysis of experimental spin-Rabi spectra measured with pEDMR and pODMR should be conducted on Fourier data obtained from Eq. (11).

In order to scrutinize the analytical description of the Rabi spectrum of a pair process given above, we can now fit the experimentally obtained Fourier transform of the electrically detected electron spin pair Rabi oscillation displayed in Fig. 5 with the analytical expressions in Eqs. (13), (20), and (25) for the Fourier transforms of an uncorrelated spin pair ensemble, $F_1(s)$, $F_2(s)$, and $F_0(s)$, respectively. It is known that weakly coupled polaron pairs in MEH-PPV do not exhibit a correlation of their local hyperfine fields,[14] so an agreement between the experimental data set and the sum of Eqs. (13), (20), and (25) is expected. Since the expressions for $F_i(s)$ are absolute, the fit of $F(s)=F_0(s)+F_1(s)+F_2(s)$ has only three fit parameters: (i) a global scaling factor of the unitless ordinate, (ii) the disorder factor Ω_R/δ_0, and (iii) a third fit variable which is the width of a homogeneous (Lorentzian) broadening of $F(s)$. This broadening is due to an experimental artifact, coming from a Fourier transformation of a finite time interval as well as the measured decay of the Rabi oscillation which is known to be due to inhomogeneities of the experimentally generated B_1 field.[23] Thus, the length (500 ns) of the experimentally recorded Rabi oscillation determines the frequency resolution of the resulting Fourier transform, while the decay ($\approx$150 ns) of the Rabi oscillation further contributes to homogeneous broadening of the experimental Fourier-transformed data.

Using the three fit variables for $F(s)$ mentioned above, we obtain a good fit of the experimental data as displayed by the blue (calculated) curve in Fig. 5. In this fit, the disorder parameter $\delta_0/\Omega_R=1.54$, with an estimated error of less than 0.2. Given the Rabi nutation frequency $\Omega_R=\gamma B_1=14.5(1.0)$ MHz, we obtain $\delta_0=22.3(3.3)$ MHz. This value is equivalent to a hyperfine broadened polaron line width of $\delta_0/\gamma=0.80(14)$ mT, a value that is in good agreement with the widths of EDMR-detected polaron spin resonances in MEH-PPV.[13,14,23] We conclude from this that the analytical expressions, Eqs. (13), (20), and (25), capture adequately the Rabi oscillations in weakly coupled spin pairs and should therefore be used for the fit of pEDMR data governed by noncorrelated spin pair ensembles.

ACKNOWLEDGMENTS

We acknowledge D. P. Waters and R. Baarda for the preparation of the MEH-PPV diode pEDMR templates. We also acknowledge the support of this work by the NSF Materials Research Science and Engineering Center (MRSEC) at the University of Utah (Grant No. DMR11-21252). C.B. further acknowledges the support through a National Science Foundation CAREER award (No. 0953225).

[1] D. Kaplan, I. Solomon, and N. F. Mott, J. Phys. (Paris) **39**, L51 (1978).
[2] C. Boehme and K. Lips, Phys. Rev. B **68**, 245105 (2003).
[3] T. W. Herring, S.-Y. Lee, D. R. McCamey, P. C. Taylor, K. Lips, J. Hu, F. Zhu, A. Madan, and C. Boehme, Phys. Rev. B **79**, 195205 (2009).
[4] S.-Y. Lee, S.-Y. Paik, D. R. McCamey, J. Hu, F. Zhu, A. Madan, and C. Boehme, Appl. Phys. Lett. **97**, 192104 (2010).
[5] C. Boehme and K. Lips, Phys. Rev. Lett. **91**, 246603 (2003).
[6] A. R. Stegner, Nat. Phys. **2**, 835 (2006).
[7] F. Hoehne, L. Dreher, H. Huebl, M. Stutzmann, and M. S. Brandt, Phys. Rev. Lett. **106**, 187601 (2011).

[8]H. Huebl, F. Hoehne, B. Grolik, A. R. Stegner, M. Stutzmann, and M. S. Brandt, Phys. Rev. Lett. **100**, 177602 (2008).
[9]W. Harneit, C. Boehme, S. Schaefer, K. Huebener, K. Fostiropoulos, and K. Lips, Phys. Rev. Lett. **98**, 216601 (2007).
[10]D. R. McCamey, H. A. Seipel, S.-Y. Paik, M. J. Walter, N. J. Borys, J. M. Lupton, and C. Boehme, Nat. Mater. **7**, 723 (2008).
[11]S. Schaefer, S. Saremi, K. Fostiropoulos, J. Behrends, K. Lips, and W. Harneit, Phys. Status Solidi B **245**, 2120 (2008).
[12]W. J. Baker, D. R. McCamey, K. J. van Schooten, J. M. Lupton, and C. Boehme, Phys. Rev. B **84**, 165205 (2011).
[13]J. Behrends, A. Schnegg, K. Lips, E. A. Thomsen, A. K. Pandey, I. D. W. Samuel, and D. J. Keeble, Phys. Rev. Lett. **105**, 176601 (2010).
[14]D. R. McCamey, K. J. van Schooten, W. J. Baker, S.-Y. Lee, S.-Y. Paik, J. M. Lupton, and C. Boehme, Phys. Rev. Lett. **104**, 017601 (2010).
[15]J. M. Lupton, D. R. McCamey, and C. Boehme, ChemPhysChem **11**, 3040 (2010).
[16]V. Rajevac, C. Boehme, C. Michel, A. Gliesche, K. Lips, S. D. Baranovskii, and P. Thomas, Phys. Rev. B **74**, 245206 (2006).
[17]A. Gliesche, C. Michel, V. Rajevac, K. Lips, S. D. Baranovskii, F. Gebhard, and C. Boehme, Phys. Rev. B **77**, 245206 (2008).
[18]C. Michel, A. Gliesche, S. D. Baranovskii, K. Lips, F. Gebhard, and C. Boehme, Phys. Rev. B **79**, 052201 (2009).
[19]F. H. L. Koppens, D. Klauser, W. A. Coish, K. C. Nowack, L. P. Kouwenhoven, D. Loss, and L. M. K. Vandersypen, Phys. Rev. Lett. **99**, 106803 (2007).
[20]J.-M. Spaeth and H. Overhof, *Point Defects in Semiconductors and Insulators: Determination of Atomic and Electronic Structure from Paramagnetic Hyperfine Interactions*, Springer Series of Materials Science, Vol. 51 (Springer-Verlag, Berlin, 2003).
[21]T. Nguyen, G. Hukic-Markosian, F. Wang, L. Wojcik, X. Li, E. Ehrenfreund, and Z. Vardeny, Nat. Mater. **9**, 345 (2010).
[22]L. Dreher, T. A. Hilker, A. Brandlmaier, S. T. B. Goennenwein, H. Huebl, M. Stutzmann, and M. S. Brandt, Phys. Rev. Lett. **106**, 037601 (2011).
[23]W. J. Baker, T. L. Keevers, J. M. Lupton, D. R. McCamey, and C. Boehme, Phys. Rev. Lett. **108**, 267601 (2012).